Plasma Modeling of a Hollow Anode for an Anode Layer Type Hall Thruster

Ken KUMAKURA*, Shinsuke YASUI, Kimiya KOMURASAKI*, and Yoshihiro ARAKAWA****

*Department of Advanced Energy, the university of Tokyo
**Department of Aeronautics and Astronautics, the university of Tokyo
Address: Hongo 7-3-1, Bunkyo, Tokyo 113-8656, JAPAN
Email: kumakura@al.t.u-tokyo.ac.jp

ABSTRACT

Structure of electrical sheath inside a hollow anode was numerically analyzed using the fully kinetic 2D3V Particle-in-Cell (PIC) and Direct Simulation Monte Carlo (DSMC) methodologies. As a result, ionization reaction in a hollow anode was found playing an important role to enhance the electron current to the anode.

NOMENCLATURE

B : magnetic induction [T]
d : anode width [m]
E : electric field strength [V/m]
e : electronic charge [C]
I : electric current [A]
m : particle Mass [kg]
n : number Density [1/m^3]
S : anode surface area [m^2]
T : temperature [eV]
t : time [s]
v : velocity [m/s]
x : position [m]
ε_0 : free space permeability constant [F/m]
λ_D : Debye length [m]
τ : mean free time [s]
ϕ : space potential [V]
R,Z,θ : cylindrical coordinate

SUBSCRIPTS

0 : anode exit
d : discharge
e : electron
i : ion
n : neutral
w : wall

INTRODUCTION

Two types of Hall thrusters are commercially used: a magnetic layer type and an anode layer type. In this research, the latter type is in consideration. The thruster configuration is shown in Fig. 1. Since channel length is shorter than channel width, plasma loss to the channel wall is smaller and lifetime is expected longer than the magnetic layer type.[1,2]

Discharge instability in anode layer type Hall thrusters would be one of the serious problems to be overcome. A hollow anode is commonly used to stabilize the discharge for these thrusters. The hollow anode makes it possible to gain enough discharge current by collecting electrons from sufficient anode surfaces.[3]

Electric potential drops sharply from the anode to the channel exit in the channel because the channel wall is made of metal and electrically connected to the cathode. The typical solution for 1-D analysis is plotted in Fig. 2. The electron number density also drops sharply inside the channel resulting in quite low number density plasma in the vicinity of anode. This is thought to cause discharge instability in this type of thruster.

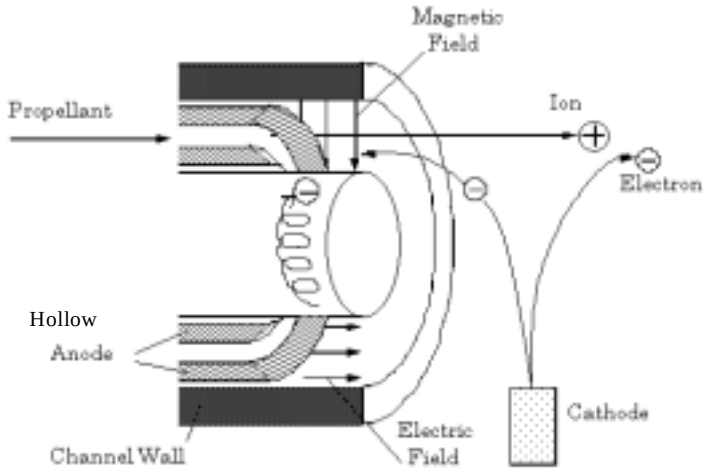

Fig. 1 Anode layer type Hall thruster.

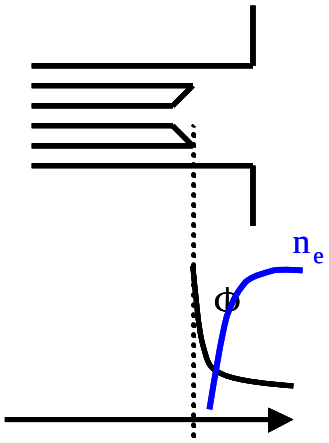

Fig. 2 Typical distributions

Through the experiments using a 1kW class anode layer type Hall thruster (Fig. 3) discharge stability was investigated.[4] Measured intensity of discharge current oscillation is shown in Fig. 4. The oscillation intensity was very sensitive to B, and stable operation regime was limited in a very narrow range of B.

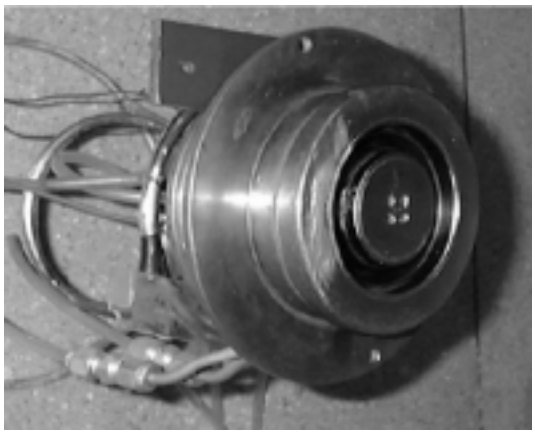

Fig. 3 A 1kW class anode-layer Hall Thruster.

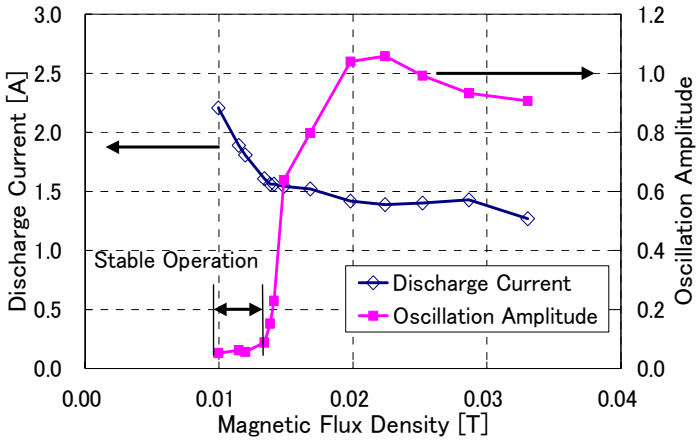

Fig. 4 Discharge current oscillation and magnetic induction.

To improve the discharge stability or to enlarge its stable operation range, electron density starvation in the vicinity of the anode surface should be avoided. Discharge current is equivalent to the total electron current on the anode as,

$$I_d = I_e = \int e n_e \bar{v}_e dS \qquad (1)$$

where S is the substantial anode surface area. As indicated in this equation, S and n_e should be large enough to realize high discharge current. The hollow anode is thought to contribute to increase S as well as n_e.

The clarification of the relationship among anode surface area, plasma measurements and sheath structure is indispensable for the prediction of thruster performance. In this research, plasma inside the hollow anode was numerically simulated using a fully kinetic 2D3V PIC-DSMC methodology.[5-7] The goal of the calculation is to model the anode sheath, which has a great effect on the range of stable discharge of anode layer type Hall thrusters, and find out a scaling law for the hollow anode design.

PHYSICAL MODEL

Typical potential distributions in a hollow anode are schematically drawn in Fig. 5.

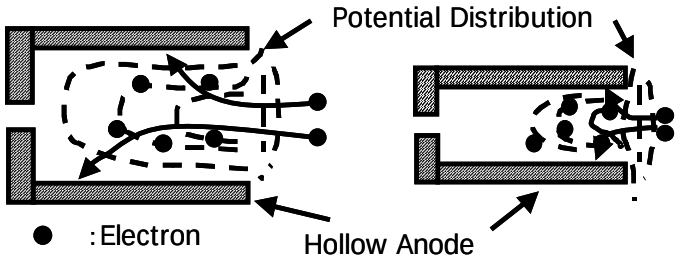

(a) (b)

Fig. 5 Schematic diagrams of the sheath structure inside a hollow anode.

When the electric field is spread deeply inside the anode as Fig. 5 (a), electrons can reach deep inside the anode and total discharge current would be high. On the other hand, when the electric field exists only in the vicinity of the anode exit as Fig. 5 (b), most of the electrons are accelerated toward the surface near the anode exit and electron current cannot be high enough without high electric potential drop nor high electron energy.

CALCULATION MODEL

Figure 6 shows the flow chart of calculation.

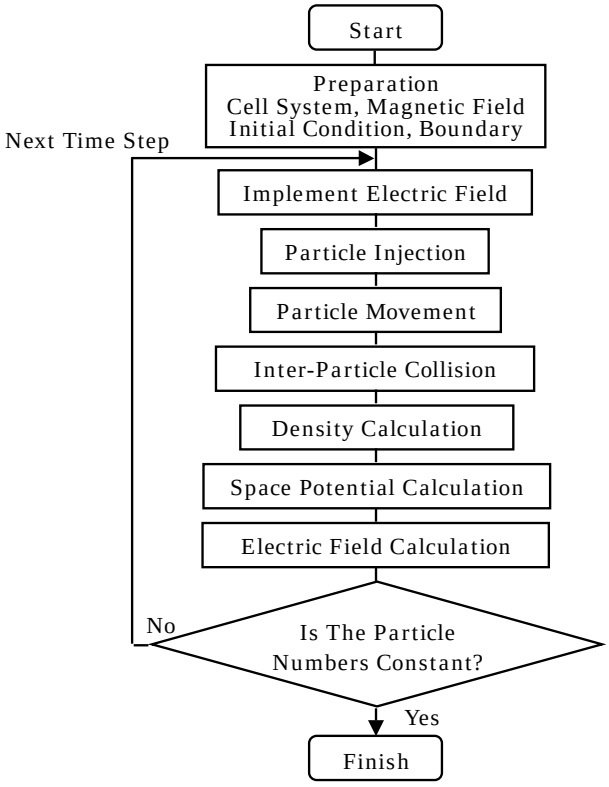

Fig. 6 A flow chart of the calculation.

All macro-particles are treated kinetically. Electric and magnetic forces are implemented via the PIC methodology and collisions are via the DSMC methodology. The cylindrical coordinate system (R, Z, θ) was applied as shown in Fig. 7. Particle's position is expressed in two-dimensional space R and Z, while its velocity is expressed in three-dimensional space. That is, particles move in all directions, but the azimuthal coordinate is always discarded.

A 36×20 orthogonal calculation grid is set, with the axial length of the cell getting smaller

toward the anode exit in order to observe the sharp fall of electron density in the vicinity of anode exit. The minimum cell length is in the same order of the Debye length.

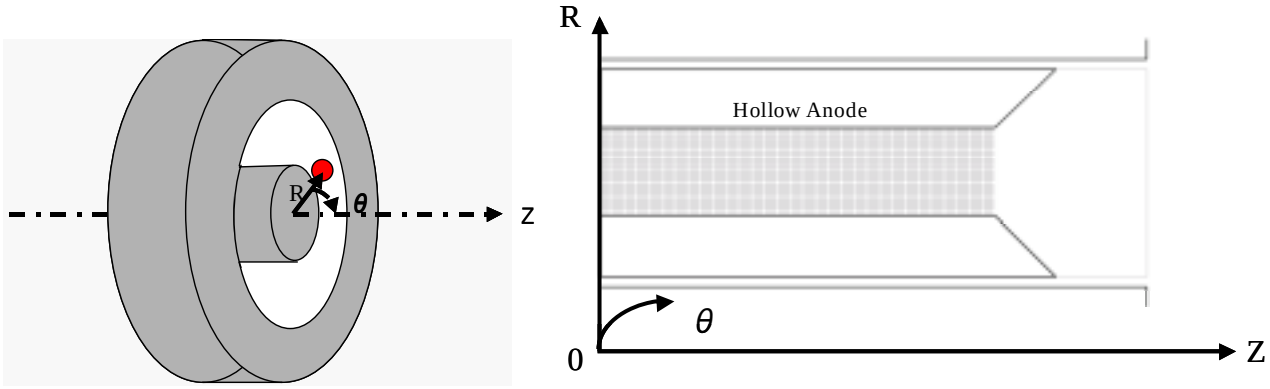

Fig. 7 The coordinate and the calculation grid.

Assumptions are listed below.

- Magnetic field lines are aligned in the radial direction uniformly inside the hollow anode and don't have axial or azimuthal components.
- Mass ratio m_n/m_e (when using Xenon as propellant) is decreased from 4×10^{-6} to 1/100, to speed up heavy particle's motion.
- Only singly charged ions are considered.

Collisions considered in this simulation are shown in Table 1. The figures in the table are examples when the particles are at their thermal velocity. The simulation time step is based on electron - neutral collision mean free time τ_{en}.

Table 1 Collisions considered in the simulation.

Collision	Mean Free Time	Relative Collision Frequency
Neutral–Neutral Scattering	3.83×10^{-5} [s]	5.32×10^{-5}
Electron–Electron Coulomb	1.527×10^{-5}[s]	1.33×10^{-4}
Electron–Neutral Elastic Scattering	2.038×10^{-9}[s]	1.00
Electron–Neutral Ionization	1.831×10^{-8}[s]	0.111
Electron–Neutral Excitation	6.683×10^{-8}[s]	3.05×10^{-2}
Electron–Ion Coulomb	2.827×10^{-7}[s]	7.21×10^{-3}

All the particles move according to the dynamic equations. The dynamic equations for charged particles are expressed as,

Electrons :
$$\begin{cases} m_e \dfrac{dv_Z}{dt} = -e(E_Z - v_\theta B_R) \\ m_e \dfrac{dv_R}{dt} = -eE_r + m_e \dfrac{v_\theta^2}{x_R} \\ m_e \dfrac{dv_\theta}{dt} = -ev_Z B_R - m_e \dfrac{v_R v_\theta}{x_R} \\ \dfrac{dx_Z}{dt} = v_z, \quad \dfrac{dx_R}{dt} = v_R \end{cases} \quad (2)$$

Ions :
$$\begin{cases} m_i \dfrac{dv_Z}{dt} = eE_Z \\ m_i \dfrac{dv_R}{dt} = eE_R \\ \dfrac{dx_Z}{dt} = v_Z \\ \dfrac{dx_R}{dt} = v_R \end{cases} \quad (3)$$

Space potential is calculated using the Poisson's equation as,

$$\frac{\partial^2 \varphi}{\partial Z^2} + \frac{1}{x_R}\frac{\partial}{\partial R}\left(x_R \frac{\partial \varphi}{\partial R} \right) = -\frac{e}{\varepsilon_0}(n_i - n_e) \qquad (4)$$

RESULTS & DISCUSSION

Firstly, the case without ionization is computed. Only electrons flow into the hollow anode. Electrons are fed from the anode exit, which is the right hand side boundary of each picture, with a T_e=10[eV] half-Maxwellian velocity distribution. The electron density on that boundary n_{e0} is a variable parameter in this calculation.

Computed electron number density and electric potential distributions are shown in Figs. 8 and 9. When n_{e0} is in the order of 10^{15}[1/m^3], electrons spread widely in the hollow anode, and electrons have reached even the far side of the anode wall. As n_{e0} gets higher, a potential drop appears and causes electrons to flow back out of the anode. As a result, electron density and electric potential dropped sharply near the exit due to the space charge limitation.

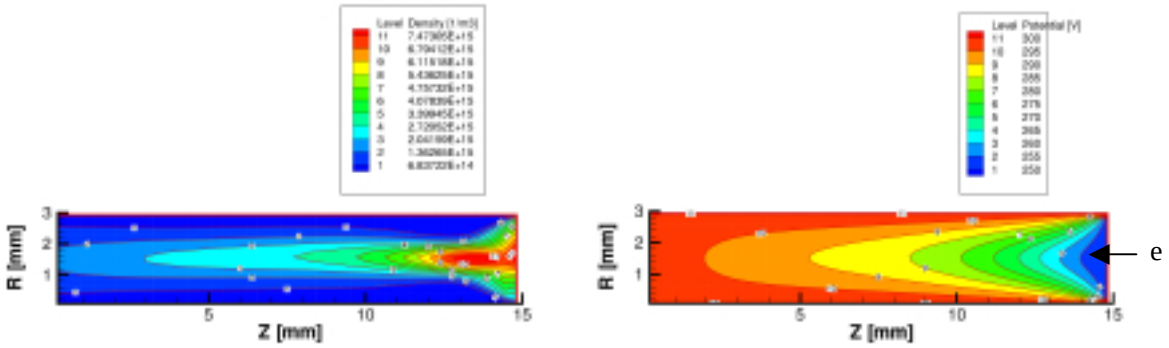

(a) Electron number density (b) Electric potential

Fig. 8 Computed distributions in the case of n_{e0}=4.92×10^{15}[1/m^3]. I_e=0.023[A].

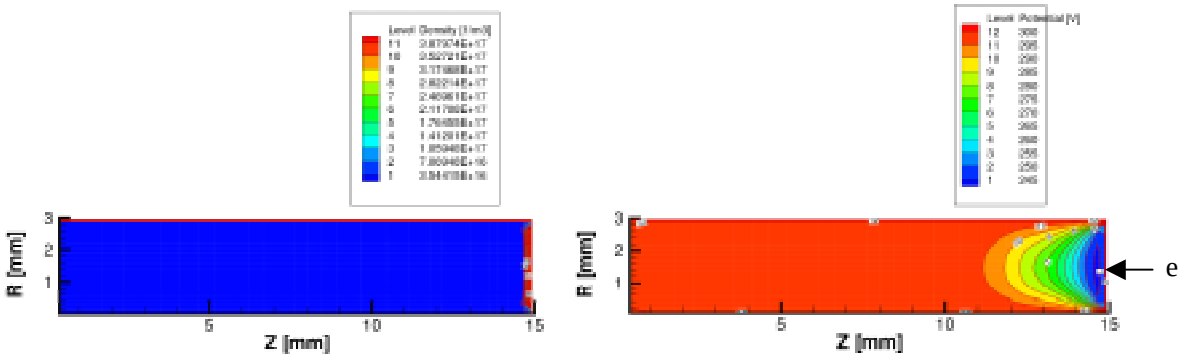

(a) Electron number density (b) Electric potential

Fig. 9 Computed distributions in the case of n_{e0}=1.36×10^{17}[1/m^3]. I_e=0.11[A].

Figure 10 shows the electron current density on the anode wall. Most of the electrons are absorbed near the anode exit, and the percentage of electrons that are absorbed on the backside wall is as small as 1.9[%].

The relation between n_{e0} and I_e is shown in Fig. 11. Although I_e was increased with n_{e0}, it was saturated due to the space charge limitation.

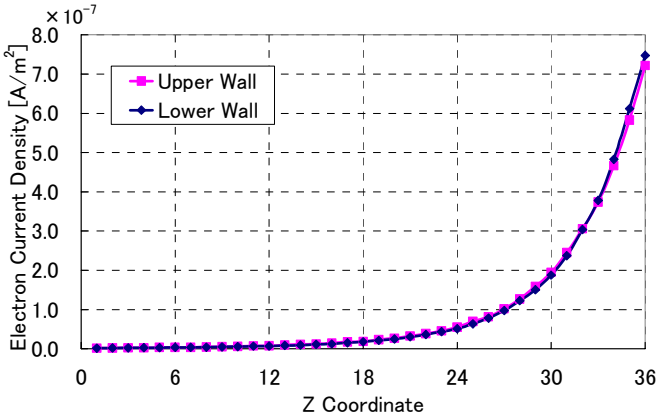

Fig. 10 Electron current density on the sidewalls of anode. n_{e0}=1.36×10^{17}[1/m^3]

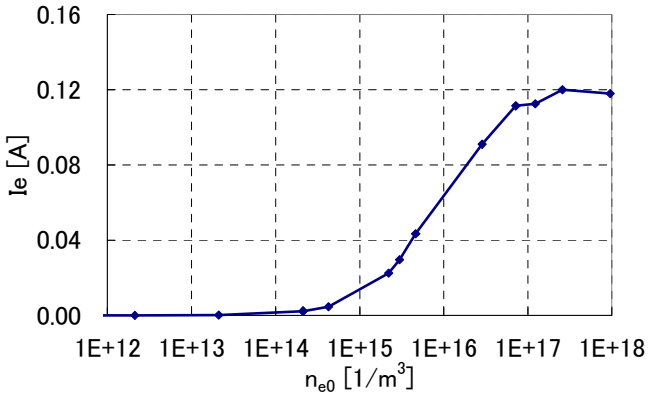

Fig. 11 Relation between n_{e0} and I_e.

The maximum discharge current was 0.12 [A]. This value is one order of magnitude smaller than actual discharge current measured in the experiment (see Fig. 4.)

The effects of boundary conditions such as electron temperature at the anode exit and the potential drop inside the hollow anode are shown in Figs. 12 and 13. When T_e is higher, electrons have higher thermal velocity on the inlet boundary, and more electrons are collected in the anode. For example, when T_e is set as high as 100 eV, I_e reached the same order of the measured one.

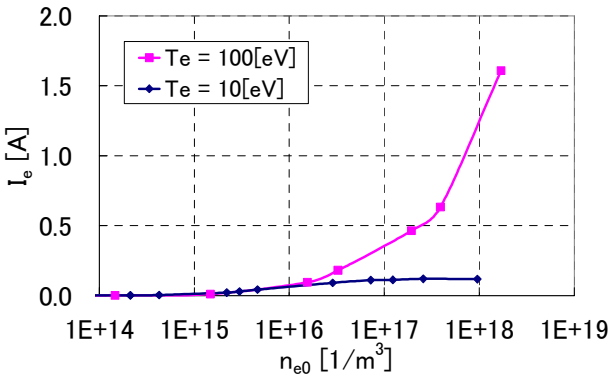

Fig. 12 Effect of electron temperature.

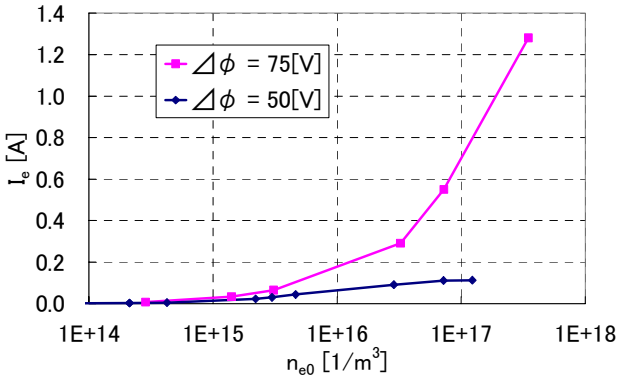

Fig. 13 Effect of potential drop.

The discharge current was increased with the potential drop Δϕ. Discharge current of 1[A] was obtained when Δϕ was as high as 75 [V],

However, increase in T_e and Δϕ implies the increase in electric power, and leads to the decrease in thrust efficiency. From the consideration of energy balance in the thruster, this

high electron temperature or large potential drop in the anode is unrealistic.

Therefore, secondly, ionization reaction in a hollow anode has been taken into account. Neutral particles enter the system from a propellant feed orifice with an initial temperature of T_n=300[K]. Colliding with the anode wall, they are reflected randomly at the wall temperature of T_w=1000[K] and gain energy. The neutral number density distribution without discharge is shown in Fig. 14.

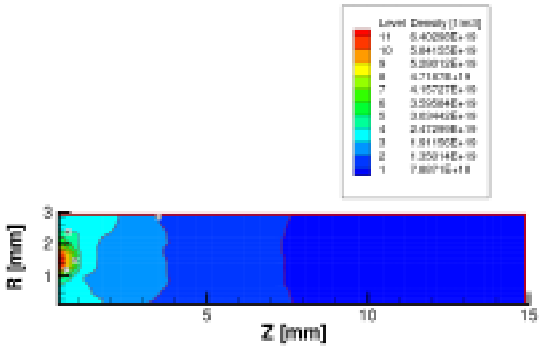

Fig. 14 Neutral number density distribution. Xe=2.0[Aeq].

Coupling the movement of neutral particles, electrons and ions, and taking into account of the collision among these particles, number density distributions and electric potential distribution are computed. Figure 15 shows the distributions in the case under nearly the same conditions as the case shown in Fig. 8. Electron current collected on the anode was I_e=1.36[A], which is about ten times larger than in the case without ionization reaction. The ion current generated inside the hollow anode was I_i=0.29[A].

The relation between n_{e0} and I_e is shown in Fig. 16.

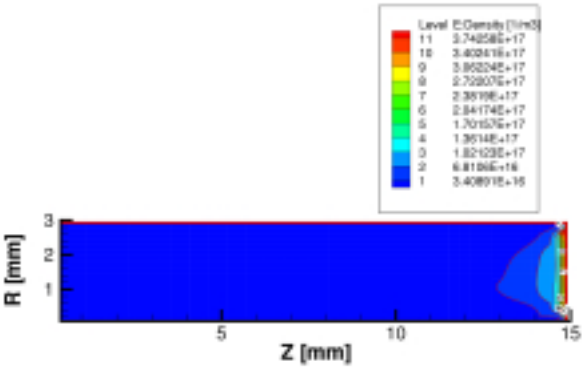

(a) Electron number density

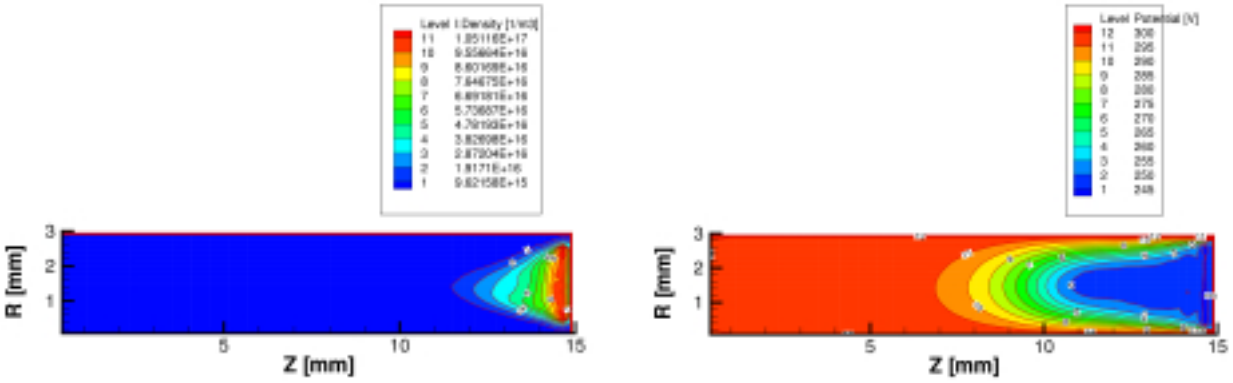

(b) Ion number density. (c) Electric potential.

Fig. 15 Computed distributions with an ionization reaction in the case of n_{e0}=2.12×10^{17}[1/m^3]. I_e=1.36 [A], I_i=0.29[A].

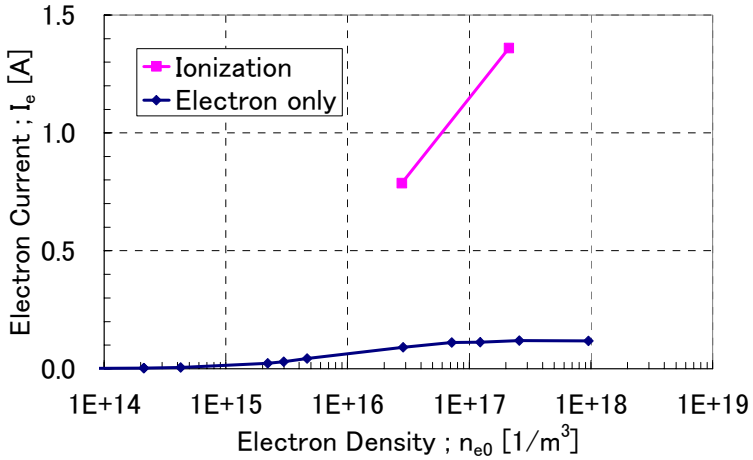

Fig. 16 Relation between n_{e0} and I_e.

CONCLUSIONS

The plasma inside a hollow anode was numerically analyzed using the PIC-DSMC methodologies. When ionization reaction is neglected, electron current collected in the anode was one order of magnitude low (I_e=0.11[A]) compared with the measured discharge current (I_e=1.0-5.0[A]). Taking ionization reaction into account, electrons collected on the anode increased to I_e=1.36[A].

REFERENCES

[1] Choueiri, E. Y., "Fundamental difference between the two Hall thruster variants", Physics of Plasmas Vol.8, No.11 November 2001.

[2] Semenkin A.V., Tverdokhlebov S.O., Garkusha V.I., Kochergin A.V., Chislov G.O., Shumkin B.V., Solodukhin A.V., Zakharenkov L.E., "Operating Envelopes of Thrusters with Anode Layer", IEPC2001-013, 27th International Electric Propulsion Conference, Pasadena, USA, October 2001.

[3] Semenkin, A., Kochergin, A., Garkusha, V., Chislov, G., Rusakov, A., "RHETT/EPDM Flight Anode Layer Thruster Development", IEPC-97-106, 25th International Electric Propulsion Conference, Cleveland, USA, August 1997.

[4] Yamamoto, N., Nakagawa, T., Komurasaki, K., Arakawa, Y., "Extending Stable Operation Range in Hall Thrusters", AIAA-2002-3953 38th AIAA/ASME/SAE/ASEE Joint Propulsion Conference & Exhibit, Indianapolis, USA, July 2002.

[5] Hirakawa, M., "Particle Simulation of Plasma Phenomena in Hall Thrusters", IEPC-95-164, 24th International Electric Propulsion Conference, Moscow, Russia, September 1995.

[6] Szabo, J. J., "Fully Kinetic Hall Thruster Modeling", IEPC-01-341, 27th International Electric Propulsion Conference, Pasadena, USA, October 2001.

[7] Szabo, J. J., "Fully Kinetic Hall Thruster Modeling of a Plasma Thruster", PhD Thesis, Massachusetts Institute of Technology, 2001.